Novel biallelic mutations in TMEM126B cause splicing defects and lead to Leigh syndrome with severe complex I deficiency

Ya Wang[1], Xiyue Zhou[1], Xiaoting Lou[2], Yuwei Zhou[1], Yaojun Xie[1], Qiyu Dong[1], Xiaojie Ying[1], Mahlatsi Refiloe Laurentinah[1], Luyi Zhang[1], Zhehui Chen[3], Dongxiao Li[3], hezhi fang[1], Jianxin Lu[1], and Yang yanling[3]

[1]Wenzhou Medical University School of Laboratory Medicine and Life Sciences
[2]Zhejiang Provincial People's Hospital
[3]Peking University First Hospital

July 8, 2022

Abstract

Leigh syndrome (LS) is one of the most common mitochondrial disease subtypes, caused by mutations in either the nuclear or mitochondrial genomes. TMEM126B was identified as a mitochondrial complex I assembly factor. Here, we identified a novel intronic mutation (c.82-2A>G) and a novel exonic insertion mutation (c.290dupT) in *TMEM126B* from a Chinese patient with clinical manifestations of LS. *In silico* predictions, minigene splicing assays and patients' RNA analyses determined that the c.82-2A>G mutation resulted in complete exon 2 skipping, and the c.290dupT mutation provoked partial and complete exon 3 skipping, leading to translational frameshifts and premature termination. Functional analysis revealed the impaired mitochondrial function in patient-derived lymphocytes due to the complex I content and assembly defect. Although *TMEM126B* mutations have been related to multi-symptoms (exercise intolerance, severe muscle weakness, hyperlactic acidemia, pure myopathy, chronic renal failure and cardiomyopathy), we found the patient carrying these two mutations developed an middle-onset LS. Altogether, this is the first report that the patient carrying *TMEM126B* mutations was diagnosed with LS. Our data uncover the functional effect and the molecular mechanism of the pathogenic variants c.82-2A>G and c.290dupT, which expand gene mutation spectrum of LS and clinical spectrum caused by *TMEM126B* mutations.

Novel biallelic mutationsin *TMEM126B* cause splicing defects and lead to Leigh syndrome with severe complex Ideficiency

Xiyue Zhou[1, #], Xiaoting Lou[2, #], Yuwei Zhou[1], Yaojun Xie[1], Qiyu Dong[1], Xiaojie Ying[1], Mahlatsi Refiloe Laurentinah[1], Luyi Zhang[1], Zhehui Chen[3], Dongxiao Li[3], Hezhi Fang[1, *], Jianxin Lyu[1, 4, *], Yanling Yang[3, *] and Ya Wang[1, *]

1 Key Laboratory of Laboratory Medicine, Ministry of Education, Zhejiang Provincial Key Laboratory of Medical Genetics, School of Laboratory Medicine and Life sciences, Wenzhou Medical University, Wenzhou 325035, Zhejiang, China;

2 Department of Genetic and Genomic Medicine, Zhejiang Provincial People's Hospital (Affiliated People's Hospital, Hangzhou Medical College), Hangzhou, Zhejiang 310014, China;

3 Department of Pediatrics, Peking University First Hospital, Beijing 100034, China;

4 Zhejiang Provincial People's Hospital, Affiliated People's Hospital of Hangzhou Medical College, Hangzhou, Zhejiang 310053, China.

[#] The authors contribute equally.

* Correspondence: Hezhi Fang (fangh@wmu.edu.cn); Jianxin Lyu (jxlu313@163.com); Yanling Yang (organic.acid@126.com); Ya Wang (yawang@wmu.edu.cn).

Abstract

Leigh syndrome (LS) is one of the most common mitochondrial disease subtypes, caused by mutations in either the nuclear or mitochondrial genomes. TMEM126B was identified as a mitochondrial complex I assembly factor. Here, we identified a novel intronic mutation (c.82-2A>G) and a novel exonic insertion mutation (c.290dupT) in *TMEM126B*from a Chinese patient with clinical manifestations of LS. *In silico* predictions, minigene splicing assays and patients' RNA analyses determined that the c.82-2A>G mutation resulted in complete exon 2 skipping, and the c.290dupT mutation provoked partial and complete exon 3 skipping, leading to translational frameshifts and premature termination. Functional analysis revealed the impaired mitochondrial function in patient-derived lymphocytes due to the complex I content and assembly defect. Although *TMEM126B* mutations have been related to multi-symptoms (exercise intolerance, severe muscle weakness, hyperlactic acidemia, pure myopathy, chronic renal failure and cardiomyopathy), we found the patient carrying these two mutations developed an middle-onset LS. Altogether, this is the first report that the patient carrying*TMEM126B* mutations was diagnosed with LS. Our data uncover the functional effect and the molecular mechanism of the pathogenic variants c.82-2A>G and c.290dupT, which expand gene mutation spectrum of LS and clinical spectrum caused by *TMEM126B*mutations.

Keywords

TMEM126B , Leigh syndrome, OXPHOS, Mitochondrial complex I, splicing defect

Introduction

Leigh syndrome (LS, MIM 256000) is the most prevalent childhood-onset mitochondrial disease, with neurodegenerative disorders as its most distinctive feature (Rahman et al., 1996). LS has a prevalence of approximately 1:40,000 and is highly genetically heterogeneous, primarily with impaired mitochondrial energy production (Darin et al., 2001). LS exhibits several different modes of inheritance (X-linked, autosomal or maternal). To data, more than 75 causing genes including both mitochondrial and nuclear genes have been identified (Schubert Baldo & Vilarinho, 2020). Although defects in each of the five oxidative phosphorylation system (OXPHOS) complexes have been observed in LS patients (Lake et al., 2016), nearly one-third of LS cases are related to complex I deficiency. Mitochondrial complex I is essential for aerobic respiratory and is located in the first of the mitochondrial oxidative respiratory chain. It oxidizes NADH, which reduces ubiquinone and transports protons through the inner mitochondrial membrane, resulting in proton driving force (Hirst, 2013). The complete assembly of complex I requires at least 45 subunits and 15 assembly factors, each of which can lead to mitochondrial complex I disruption and ultimately cause diverse human diseases including neurodegenerative diseases, aging, mitochondrial disorder and etc (Formosa et al., 2018; Mimaki et al., 2012; Schapira, 1993; Tinker et al., 2021).

TMEM126B (MIM 615533) is a 7968-bp gene containing five exons that encodes a component of mitochondrial complex I intermediate assembly (MCIA) complex, which is required for assembly of complex I but is not part of the mature complex (Heide et al., 2012). Mutations in*TMEM126B* would cause an isolated mitochondrial complex I deficiency and result in various clinical phenotypes such as exercise intolerance, muscle weakness, hyperlactic acidemia, hypertrophic cardiomyopathy and renal tubular acidosis (Alston et al., 2016; Sánchez-Caballero et al., 2016; Theunissen et al., 2017). To date, ten patients with a total of four mutations in *TMEM126B* have been reported worldwide, but all patients reported had a normal in neurological presentation (Alston et al., 2016; Sánchez-Caballero et al., 2016; Theunissen et al., 2017). Notably, the genetic spectrum of the *TMEM126B* mutations in China remains unclear.

In this study, using next-generation sequencing in a Chinese patient manifested with LS, we identified two novel heterozygous mutations of *TMEM126B* (c.82-2A>G and c.290dupT). Bioinformatics analysis and functional assays revealed that c.82-2A>G mutation caused complete exon 2 skipping and c.290dupT induced partial and complete exon 3 skipping. Patient-derived lymphoblastoid cells carrying biallelic mutations

exhibited complex I content and assembly defect and mitochondrial dysfunction. Our findings uncovered the functional effect and the molecular mechanism of the pathogenic *TMEM126B* variants c.82-2A>G and c.290dupT, which not only expand the gene mutation spectrum of LS, but also expand the clinical spectrum caused by *TMEM126B* mutations.

Material and methods

Patient

The patient was admitted to the Department of Pediatrics at Peking University First Hospital and the clinical diagnosis of LS was established in accordance with previously published criteria (Rahman et al., 1996). The study received ethical review from Peking University First Hospital (2017-217) and obtained informed consent from the participant's legal guardian and family members.

Variants validation

To elucidate the disease-causing genes, we obtained venous whole blood samples from the individual and her parents for whole-exome and mitochondrial genomic sequencing. According to the instructions of the manufacturer, the patient's and parents' DNA were extracted using the DNA extraction kit (Beyotime Biotechnology, China). Whole-exome and mitochondrial genomic sequencing were performed by Aegicare (China). The candidate disease-causing gene was screened according to the criteria mentioned before (Richards et al., 2015). Total DNA extracted from patient and the parents was amplified by 2×Taq Master Mix (Vazyme, China) according to the manufacturer's instruction, and the variants were verified by sanger sequencing. The primers are as follows: DupT-F: TTTGTTTACT GTCCTATCTTAAGCAC, dupT-R: ACCTGATTAGGAGGATTGTTGC, 82-2-F: AAG CCAATGT CTAACAGATAAT, 82-2-R: CTTGTTTC-CCCCATTCTT. Then segregation study was performed base on the mendelian law.

Bioinformatics analyses of variants

To characterize the population frequency and the pathogenicity of the variants, we predicted the population allele frequency of the variants using 1000 genomes (https://www.internationalgenome.org/), gnomAD (https://gnomad.broadinstitute.org/) and ExAc allele frequency (http://exac.broadinstitute.org) based on the previous mentioned (Gudmundsson et al., 2021; Kobayashi et al., 2017; Zheng-Bradley & Flicek, 2017). dbSNP (https://www.ncbi.nlm.nih.gov/snp/), Clinvar (https://www. ncbi.nlm.nih.gov/clinvar/) and HGMD (Human Gene Mutation Database, http://www. hgmd.cf.ac.uk/ac/index.php) were used to predict the pathogenicity of the variants (Landrum et al., 2018; Sherry et al., 2001; Stenson et al., 2014). Pathogenicity of both variants was analyzed according to the American College of Medical Genetics and Genomics guidelines (Richards et al., 2015). MetaDome (https://stuart.radboudumc.nl/metadome/) (Wiel et al., 2019) combined with NCBI-BLAST (https:// blast.ncbi.nlm.nih.gov/Blast.cgi) to analyze the variant tolerance of *TMEM126B* exon 2 as well as exon 3 and amino acid conservation among mammals. Alternative splice site predictor (http://wangcomputing.com/assp/) (Wang & Marín, 2006) and exonic splicing regulation (http://krainer01.cshl.edu/tools/ESE2/) (Cartegni et al., 2003) to predict the effect of two variants on*TMEM126B* mRNA splicing.

Minigene construction and expression

The minigene expression plasmids were constructed as previously reported (Beck et al., 2013) and *in vitro* splicing confirmation was performed follow before (Volodarsky et al., 2015). pSPL3, a cloning expression plasmid, was purchased from Fenghui Biotechnology (China). Briefly, the vector was cleaved with *Bam* HI (Takara Bio, USA) and*Eco* RI (Takara Bio), and then ligated the DNA segment containing the two mutation sites to the pSPL3 vector using T4 ligase (NEB, USA) following the manufacturer's instruction. The primers were as follows: dup-F: 5'-CGCTCGAGTTTGTTTACTG TCCTATCTTAAGCAC-3', dup-R: 5'-CGGGATCCACCTGATTAGGAGGATTGTTGC-3', 82-2-F: 5'-CGCTCGAGAAGCCAATGTCTAACAGATAAT-3', 82-2-R: 5'-CGGGATCCCTTGTTTCCCCCATT CTT-3'.

Cell culture

Immortalized lymphocytes derived from II-1 and healthy controls were conducted using epstein-barr virus procured from B95-8 cells (Cell Bank of the Chinese Academy of Science, China) as mentioned before (Lou et al., 2018). Immortalized B lymphocytes were culture in Roswell Park Memorial Institute (RPMI) 1640 medium (Sigma-Aldrich) supplement with 10% fetal bovine serum (Sigma-Aldrich), 1% (v/v) penicillin-streptomycin (Beyotime Biotechnology) and 0.25 μg/mL amphotericin B (Beyotime Biotechnology). HEK293T cells (Cell Bank of the Chinese Academy of Science) were cultured in Dulbecco's Modified Eagle Medium (DMEM) medium (Sigma-Aldrich) supplement with 12% fetal calf serum (Sigma-Aldrich) and 1% (v/v) penicillin-streptomycin and 0.25 μg/mL amphotericin B. All cells were cultured in 37 incubator with 5% CO_2.

Transfection and RT-PCR analysis

The minigene plasmid transfected into HEK293T cells with lipofectamine 3000 reagent (Thermo Fisher Scientific, USA) based on manufacturer's instruction. After 48h, collected the cells and then performed RT-PCR to evaluate the mRNA splicing. Briefly, total RNA was extracted using TRIzol reagent (Sigma-Aldrich) and then reverse transcribed to cDNA by reverse transcription kit (Vazyme) according to the instruction. PCR was performed to amplify the fragment containing the mutant site. All primers were listed below: forward: 5'- ATGGTGGTGTTCGGGTATGA-3', reverse: 5'-AGCGTCTGAACAG GAAGTTTG-3' (for lymphocytes, exon 1-3); forward: 5'-GAAGCGCCCAAGGTTTTCAA-3', reverse: 5'-ACTATGCCAATCAGTGAGCTTCT-3' (for lymphocytes, exon 2-4); dSD-F: 5'-TCTGAGTC ACCTGGACAACC-3', dSA-R: 5'-ATCTCAGTGGTATTTGTGAGC-3' (for HEK293T cells). Agarose gel electrophoresis (BioFroxx, Germany) was used to separate the segment of PCR products. Then the sequence of each DNA product was determined by sanger sequence.

Blue native polyacrylamide gel electrophoresis

Blue native polyacrylamide gel electrophoresis (BN-PAGE) was conducted as mentioned before (Wei et al., 2020). For mitochondrial supercomplexes, 1% digitonin (Sigma-Aldrich) was used to dissolve the membrane protein from patient and controls, then 3.5%-16% gradients polyacrylamide gel to separate the supercomplexes. For mitochondrial complexes, 1% dodecyl maltoside (DDM, Sigma-Aldrich) was used and then 3%-11% gradient polyacrylamide gel to separate the complexes. The proteins were transferred on the PVDF membrane (Bio-Rad, USA), blocked with 5% no-fatty acid milk (Mengniu, China), incubated with the first and second antibodies, and detected the protein signals. The following antibodies were used: anti-Grim19 (1:1000, Sigma-Aldrich), anti-SDHA (1:3000, Sigma-Aldrich), anti-UQCRC2 (1:2000, Sigma-Aldrich), anti-MT-COI (1:2000, Sigma-Aldrich), anti-ATP5A (1:3000, Sigma-Aldrich), anti-NDUFB6 (1:2000, Sigma-Aldrich), anti-NDUFS3 (1:2000, Sigma-Aldrich), anti-TOM70 (1:2000, Proteintech, China), anti-mouse IgG HRP linked (1:2000, Cell Signaling Technology, USA), anti-rabbit IgG HRP linked (1:2000, Cell Signaling Technology), anti-mouse IgG, AP (1:2000, Cell Signaling Technology).

Oxygen consumption rate

Oxygen consumption rate was performed as before (Wei et al., 2020). In short, 5×10^6 immortalized lymphocytes from the candidate and the age-matched healthy controls were rapidly and gently harvested and then added to the oxygraphy-2k detector (Oroboros, Austria). Oligomycin (0.1 mg/mL, Sigma-Aldrich) was used to detect the ATP-linked respiration. Carbonyl cyanide 4-(trifluoromethoxy) phenylhydrazone (0.1mM, Sigma-Aldrich) was for the maximal respiration and the reserve respiratory capacity.

Cellular ATP content and mitochondrial ROS level detection

Cellular ATP and mitochondrial ROS content were measured by ATP bioluminescent assay kit (Sigma-Aldrich) and MitoSOX Red reagent (Thermo Fisher Scientific) following the manufacturer's instruction, respectively (Wei et al., 2020). For cellular ATP content measurement, immortalized lymphocytes from patient and age-matched healthy controls were collected and s resuspended with filtered ultrapure water. Then added the cell suspension to the ATP-releasing solution and detected the autofluorescence. The protein

concentration of the samples was measured with the BCA protein concentration assay kit (Thermo Fisher Scientific) as a calibration. For the mitochondrial ROS level detection, immortalized lymphocytes from patients and age-matched healthy controls were collected and resuspended in working solution containing 5uM MitoSOX reagent. Then incubated at 37degC for 10 mins at dark, gently washed cells and detected the fluorescence.

Results

Clinical manifestation and genetics analysis

The individual (II-1) was born into nonconsanguineous healthy Chinese family with a normal gestational and delivery record. She fell the development milestone, with instability in walking at the age of 12 months, and received recovery training for two months, however, no improvement in her symptoms. She developed uninterrupted strabismus in her left eye at the age of 2 years. Imaging tests showed negative brain magnetic resonance imaging (MRI) and electroencephalogram (EEG). She was consulted in the Department of Genetic Metabolism at Peking University First Hospital when she was three years and two months old. The candidate walked unsteadily, with weak muscular strength, reduced muscle tension, malnutrition but well developed reflexes and mental response. The face of patient was yellow, with yellow palms and feet, and the back of the neck was ciliated. Metabolic investigation showed increased blood lactate (3.14, normal range 0.50-2.20 mM) and β- hydroxybutyric acid (1.18, normal range 0.02-0.27 mM). Amino acid and acylcarnitine profile analysis showed there were no significant abnormal findings. Other tests showed increased aspartate amino acid transferase (42.2, normal range 0.0-35.0 U/L), lactate dehydrogenase (247.3, normal range 109.0-245 U/L) and ∝-hydrobutyrate dehydrogenase (260.8, normal range 90.0-250.0 U/L), indicating an abnormal liver function. MRI demonstrated symmetrical abnormal signals in bilateral cerebral peduncles, and abnormal signals in the cerebral bridge with adenoid hypertrophy (Figure 1A). Electromyogram/evoked potentials test (EMG/EP) revealed that left gastrocnemius nerve had sensory conduction abnormalities. Echocardiogram was normal. She was established the diagnosis of LS according to the standard criteria (Rahman et al., 1996). Next-generation sequencing was performed to detect the disease-causing gene of the probing, after the filtering with established criteria (Wei et al., 2020), a novel splice site variant (c.82-2A>G, intron 1) and a novel insertion variant (c.290dupT, exon 3) in *TMEM126B* (NM_018480.7) were identified and no clinically significant mitochondrial genomic-related variants were detected. Segregation analysis confirmed that c.82-2A>G was maternal inherited while c.290dupT was paternal (Figure 1B and 1C).

A comprehensive*in silico* analysis ofc.82-2A>G and c.290dupT

To investigate the potential pathogenicity of the above two variants (c.82-2A>G and c.290dupT), we performed a series of bioinformatics analyses. As shown in Figure 2A, both exon 2 and exon 3 of *TMEM126B* are conserved across the species and mutations in exon 3 is prone to intolerance by using the MetaDome web tool (Wiel et al., 2019), and the p.98K seems intolerance and highly conservative. The prediction for the pathogenicity in several databases showed c.82-2A>G was like pathogenic and c.290dupT was pathogenic, the allele frequency of c.82-2A>G in gnomAD was extremely low (0.0006), and neither of them had record in several population variation frequency and pathogenicity prediction databases (Figure 2B). ASSP (Alternative Splice Site Predictor) (Wang & Marín, 2006) indicates that the c.82-2A>G mutation may destroy original splice constitutive acceptor, while the frameshift mutation c.290dupT may create a new splice constitutive acceptor (Figure 2C). ESE finder (exonic splicing enhancers) predicts the c.82-2A>G variant resulted in a decrease in the SRp40 binding sequence score, and the c.290dupT variant leads to increased SRp40 binding sequence score and loss of SRp55 binding sequence (Figure 2D). Taken together, these results indicate that both of these mutations (c.82-2A>G and c.290dupT) are disease-causing and affect pre-mRNA splicing.

Identification of variants affecting *TMEM126B* splicing by using a minigene splicing assay

To explore whether the c.82-2A>G and c.290dupT variants influence mRNA splicing, we conducted an exon trapping assay based on pSPL3 plasmids (Figure 3A). RT-PCR and Sanger sequencing showed that both the empty pSPL3 control and c.82-2G mutant constructs gave rise to a 263-bp PCR fragment missing exon 2 of*TMEM126B* gene, whereas the wild-type c.82-2A yielded a RT-PCR product of 385-bp containing exon

2 (Figure 3B and 3C), which indicated that c.82-2A>G mutation destroyed the original splice acceptor site and resulted in full exon 2 skipping. The plasmid constructs of both wild-type c.290T and mutant c.290dupT expressed three transcripts, including a transcript without exon 3, a transcript with 103-bp deletion of exon 3 and a transcript containing exon 3 but with one base (T) duplication (Figure 3D and 3E). Quantitative analysis showed that natural partial and complete exon 3 skipping were weak in wild-type c.290T construct, but significantly increased in mutant c.290dupT (Figure 3F). Altogether, our data suggested that c.82-2A>G mutation caused complete exon 2 skipping and c.290dupT induced partial and complete exon 3 skipping.

Confirmation of variant-induced spliceogenicity inpatient-derivedlymphocytes

To assess the physiologic relevance of the splicing defects revealed by the minigene assay, we analyzed the splicing pattern of *TMEM126B* in patient-derived lymphocytes. RT-PCR using primers specific to exons 1 and 3 spanning the variant c.82-2A>G generated a PCR product with complete exon 2 skipping in patient-derived sample (Figure 4A and 4B), resulting in a 40 amino-acid deletion with a subsequent frame-shift from codon 28 and premature termination at position 58 in exon 3 (Figure 4C), thus leading to nonsense-mediated mRNA decay. Agarose gel analysis and Sanger sequencing of the RT-PCR products generated from patient-derived mRNA using primers specific to exons 2 and 4 detected a full-length transcript carrying the c.290dupT in exon 3 and a shorter mRNA with the c.290dupT and 103-bp deletion of exon 3 (Figure 4D and 4E). Both of the above transcripts were predicted to cause frameshift and premature termination (Figure 4F), which would likely lead to transcript elimination via the nonsense-mediated decay pathway. Whereas very little levels of*TMEM126B* cDNA lacking 103-bp from exon 3 could be detected in control lymphocytes, further suggesting c.290dupT induced splicing defects. These results obtained from patient-derived RNA samples were in agreement with the minigene data.

Mitochondrial complex I content and assembly defect and mitochondrial dysfunction in patient- derived lymphocytes

To validate the pathogenic role of c.82-2A>G and c.290dupT variants in *TMEM126B* , OXPHOS supercomplexes and complexes were tested in patient-derived lymphocytes. The results indicated that the content of complex I was markedly decreased in patient-derived immortalized lymphocytes compared with normal controls. Moreover, supercomplex $CI/III_2/IV$ assembly was blocked, while lower assembly intermediate appeared to accumulate notably (Figure 5A and 5B). Mitochondrial respiratory chain complexes are involved in maintaining proper mitochondrial function, and we then investigated mitochondrial functions in patient-derived immortalized lymphocytes. As shown in Figure 5C, patient-derived lymphocytes showed a general decrease in cellular respiratory capacity, including basal, ATP-linked respiration, maximal respiration, and spare respiration capacity compared to controls. Cellular ATP content of patient-derived lymphocytes was significantly decreased, whereas the mitochondrial ROS level was increased (Figure 5D and 5E). Together, these results demonstrated that mitochondrial OXPHOS function was severely impaired in patient-derived lymphocytes carrying mutations of c.82-2A>G and c.290dupT.

Literature review and the combination clinical phenotype of*TMEM126B* mutations

In order to study the overall clinical phenotypic spectrum caused by*TMEM126B* (NM_018480.7) mutations, all published literatures were reviewed (Alston et al., 2016; Sanchez-Caballero et al., 2016; Theunissen et al., 2017). Upset-plot (Lex et al., 2014) unraveled recurrent clinical phenotypes mainly including muscle symptoms (100%, 10/10), developmental delay (30%, 3/10), and visual problems (20%, 2/10) (Figure 6A). The newly identified individual (II-1) was diagnosed with LS with the characteristic MRI presentations, bilateral abnormal signal in cerebral peduncle and pons (Figure 6A). All point mutations and frameshift mutations reported before are included here for the genotype spectrum study (Figure 6B). Interestingly, except our report, none of the mutation affected exon 2. Overall genotype-phenotype correlation of *TMEM126B* was analyzed by reviewing all the published literature, the enzymatic activity of the complex I in all patients decreased, and the phenotypes were various mainly the muscle intolerance, development delay (Table 1). II-1 was the only individual presented neurological symptoms and diagnosed as Leigh syndrome.

Discussion

In this study, we described two novel heterozygous mutations of *TMEM126B* (c.82-2A>G and c.290dupT) from a Chinese patient manifested with LS. *In silico* predictions, minigene splicing assays and patients' RNA analyses were combined to determine that the c.82-2A>G mutation resulted in exon 2 completely skipped, and that the c.290dupT mutation caused an increase of partial and complete exon 3 deletion transcripts, which would lead to frameshift and premature termination. Patient-derived immortalized lymphocytes carrying biallelic mutations exhibited complex I content and assembly defect and mitochondrial dysfunction. To the best of our knowledge, this is the first report that *TMEM126B* mutations cause LS.

TMEM126B was identified as the part of MCIA complex to co-migrate with other MCIA complex components (NDUFAF1, ECSIT, and ACAD9) by complexome profiling (Heide et al., 2012). The defect of each components can cause heterogeneous clinical phenotypes. For example, mutations in *NDUFAF1* mostly associated with cardiological symptoms (Dunning et al., 2007; Elisa Fassone et al., 2011), including Wolff-Parkinson-White syndrome and hypertrophic cardiomyopathy. Genetically deficit in *ACAD9* commonly linked to cardiac symptoms, neurological symptoms, and severe lactic acidosis (E. Fassone et al., 2011; Schiff et al., 2015). Mendelian mutations in *ECSIT* gene has not yet reported. Individuals carrying *TMEM126B* mutations mainly presented with exercise intorlance, muscle weakness, hyperlactic acidemia, pure myopathy, chronic renal failure and cardiomyopathy (Alston et al., 2016; Sanchez-Caballero et al., 2016; Theunissen et al., 2017). Notably, the clinical phenotypes of our patient are consistent with those of patients carrying *TMEM126B* mutations previously reported, except for chronic renal failure and cardiomyopathy (Table 1). Chronic renal failure is not a necessary symptom to diagnose mitochondrial diseases. Significantly, our patient show a more severe neurological symptoms with clinical presentation consistent with LS. Overall, we believe that patients with *TMEM126B* mutations may exhibit high clinical heterogenicity. The combination of clinical and molecular diagnosis are required for the diagnosis of *TMEM126B* mutation-related mitochondrial diseases.

In silico analysis indicateed that the c.82-2A>G mutation located 2bp before exon 2 could lead to the loss of the original 3'splice acceptor site, while the c.290dupT mutation located exon 3 might create a new constitutive splice acceptor site. In *vitro* experiments verified that c.82-2A>G mutation led to complete exon 2 skipping and c.290dupT caused an increase of transcripts with partial and complete deletion of *TMEM126B* exon 3. Mutations that located in exonic splicing enhancer (ESE) region are thought to prevent serine and arginine-rich (SR) proteins from binding to ESE sequence motifs, which induced exon skipping. Results of ESE finder software suggested that c.290dupT mutation may disrupt a putative SRp55 binding site, thus increasing the proportion of abnormal splicing transcripts. Further functional study indicated that patient-derived immortalized lymphocytes exhibited a global mitochondrial dysfunction with decreased mitochondrial respiratory capacity, reduced ATP content and increased mitochondrial ROS levels due to the complex I content and assembly defect. Unlike previous reports, biallelic mutations in our patient caused the complete deletion of exon 2 and the partial truncation of exon 3 of *TMEM126B* , which resulted in a more severe *TMEM126B* defect, leading to a more severe complex I deficiency and brain phenotypes.

In summary, we identify *TMEM126B* as a novel disease-causing gene resulting in LS with obvious neurological symptoms, and report two novel *TMEM126B* mutations (c.82-2A>G and c.290dupT) that cause splicing defects and lead to mitochondrial dysfunction due to the severe complex I deficiency. Our study expands the genetic mutation spectrum of LS and the clinical spectrum caused by *TMEM126B* mutations.

Acknowledgements

This work was supported by grant of the National Natural Science Foundation of China (Grant Number: 81830071). We wish to thank patient and family participated in the research.

Conflict of interest statement

The authors declare that they have no conflict of interest.

Data availability statement

The data that support this study are available from the corresponding author upon reasonable request.

Reference

Alston, C. L., Compton, A. G., Formosa, L. E., Strecker, V., Olahova, M., Haack, T. B., . . . Taylor, R. W. (2016). Biallelic Mutations in TMEM126B Cause Severe Complex I Deficiency with a Variable Clinical Phenotype. *Am J Hum Genet* , *99* (1), 217-227. https://doi.org/10.1016/j.ajhg.2016.05.021

Beck, B. B., Baasner, A., Buescher, A., Habbig, S., Reintjes, N., Kemper, M. J., . . . Hoppe, B. (2013). Novel findings in patients with primary hyperoxaluria type III and implications for advanced molecular testing strategies. *Eur J Hum Genet* , *21* (2), 162-172. https://doi.org/10.1038/ejhg.2012.139

Cartegni, L., Wang, J., Zhu, Z., Zhang, M. Q., & Krainer, A. R. (2003). ESEfinder: A web resource to identify exonic splicing enhancers.*Nucleic Acids Res* , *31* (13), 3568-3571. https://doi.org/10.1093/nar/gkg616

Darin, N., Oldfors, A., Moslemi, A. R., Holme, E., & Tulinius, M. (2001). The incidence of mitochondrial encephalomyopathies in childhood: clinical features and morphological, biochemical, and DNA abnormalities.*Ann Neurol* , *49* (3), 377-383.

Dunning, C. J., McKenzie, M., Sugiana, C., Lazarou, M., Silke, J., Connelly, A., . . . Ryan, M. T. (2007). Human CIA30 is involved in the early assembly of mitochondrial complex I and mutations in its gene cause disease. *Embo j* , *26* (13), 3227-3237. https://doi.org/10.1038/sj.emboj.7601748

Fassone, E., Taanman, J.-W., Hargreaves, I. P., Sebire, N. J., Cleary, M. A., Burch, M., & Rahman, S. (2011). Mutations in the mitochondrial complex I assembly factor NDUFAF1 cause fatal infantile hypertrophic cardiomyopathy. *48* (10), 691-697. https://doi.org/10.1136/jmedgenet-2011-100340 %J Journal of Medical Genetics

Fassone, E., Taanman, J. W., Hargreaves, I. P., Sebire, N. J., Cleary, M. A., Burch, M., & Rahman, S. (2011). Mutations in the mitochondrial complex I assembly factor NDUFAF1 cause fatal infantile hypertrophic cardiomyopathy. *J Med Genet* , *48* (10), 691-697. https://doi.org/10.1136/jmedgenet-2011-100340

Formosa, L. E., Dibley, M. G., Stroud, D. A., & Ryan, M. T. (2018). Building a complex complex: Assembly of mitochondrial respiratory chain complex I. *Semin Cell Dev Biol* , *76* , 154-162. https://doi.org/10.1016/j.semcdb.2017.08.011

Gudmundsson, S., Singer-Berk, M., Watts, N. A., Phu, W., Goodrich, J. K., Solomonson, M., . . . O'Donnell-Luria, A. (2021). Variant interpretation using population databases: Lessons from gnomAD.*Hum Mutat* . https://doi.org/10.1002/humu.24309

Heide, H., Bleier, L., Steger, M., Ackermann, J., Drose, S., Schwamb, B., . . . Brandt, U. (2012). Complexome profiling identifies TMEM126B as a component of the mitochondrial complex I assembly complex. *Cell Metab* , *16* (4), 538-549. https://doi.org/10.1016/j.cmet.2012.08.009

Hirst, J. (2013). Mitochondrial complex I. *Annu Rev Biochem* ,*82* , 551-575. https://doi.org/10.1146/annurev-biochem-070511-103700

Kobayashi, Y., Yang, S., Nykamp, K., Garcia, J., Lincoln, S. E., & Topper, S. E. (2017). Pathogenic variant burden in the ExAC database: an empirical approach to evaluating population data for clinical variant interpretation. *Genome Med* , *9* (1), 13. https://doi.org/10.1186/s13073-017-0403-7

Lake, N. J., Compton, A. G., Rahman, S., & Thorburn, D. R. J. A. o. n. (2016). Leigh syndrome: one disorder, more than 75 monogenic causes.*79* (2), 190-203.

Landrum, M. J., Lee, J. M., Benson, M., Brown, G. R., Chao, C., Chitipiralla, S., . . . Maglott, D. R. (2018). ClinVar: improving access to variant interpretations and supporting evidence. *Nucleic Acids Res* , *46* (D1), D1062-d1067. https://doi.org/10.1093/nar/gkx1153

Lex, A., Gehlenborg, N., Strobelt, H., Vuillemot, R., & Pfister, H. (2014). UpSet: Visualization of Intersecting Sets. *IEEE Trans Vis Comput Graph* , *20* (12), 1983-1992. https://doi.org/10.1109/tvcg.2014.2346248

Lou, X., Shi, H., Wen, S., Li, Y., Wei, X., Xie, J., . . . Lyu, J. (2018). A Novel NDUFS3 mutation in a Chinese patient with severe Leigh syndrome. *J Hum Genet* , *63* (12), 1269-1272. https://doi.org/10.1038/s10038-018-0505-0

Mimaki, M., Wang, X., McKenzie, M., Thorburn, D. R., & Ryan, M. T. (2012). Understanding mitochondrial complex I assembly in health and disease. *Biochim Biophys Acta* , *1817* (6), 851-862. https://doi.org/10.1016/j.bbabio.2011.08.010

Rahman, S., Blok, R. B., Dahl, H. H., Danks, D. M., Kirby, D. M., Chow, C. W., . . . Thorburn, D. R. (1996). Leigh syndrome: clinical features and biochemical and DNA abnormalities. *Ann Neurol* , *39* (3), 343-351. https://doi.org/10.1002/ana.410390311

Richards, S., Aziz, N., Bale, S., Bick, D., Das, S., Gastier-Foster, J., . . . Rehm, H. L. (2015). Standards and guidelines for the interpretation of sequence variants: a joint consensus recommendation of the American College of Medical Genetics and Genomics and the Association for Molecular Pathology. *Genet Med* , *17* (5), 405-424. https://doi.org/10.1038/gim.2015.30

Sanchez-Caballero, L., Ruzzenente, B., Bianchi, L., Assouline, Z., Barcia, G., Metodiev, M. D., . . . Rotig, A. (2016). Mutations in Complex I Assembly Factor TMEM126B Result in Muscle Weakness and Isolated Complex I Deficiency. *Am J Hum Genet* , *99* (1), 208-216. https://doi.org/10.1016/j.ajhg.2016.05.022

Schapira, A. H. (1993). Mitochondrial complex I deficiency in Parkinson's disease. *Adv Neurol* , *60* , 288-291.

Schiff, M., Haberberger, B., Xia, C., Mohsen, A. W., Goetzman, E. S., Wang, Y., . . . Vockley, J. (2015). Complex I assembly function and fatty acid oxidation enzyme activity of ACAD9 both contribute to disease severity in ACAD9 deficiency. *Hum Mol Genet* , *24* (11), 3238-3247. https://doi.org/10.1093/hmg/ddv074

Schubert Baldo, M., & Vilarinho, L. (2020). Molecular basis of Leigh syndrome: a current look. *Orphanet J Rare Dis* , *15* (1), 31. https://doi.org/10.1186/s13023-020-1297-9

Sherry, S. T., Ward, M. H., Kholodov, M., Baker, J., Phan, L., Smigielski, E. M., & Sirotkin, K. (2001). dbSNP: the NCBI database of genetic variation. *Nucleic Acids Res* , *29* (1), 308-311. https://doi.org/10.1093/nar/29.1.308

Stenson, P. D., Mort, M., Ball, E. V., Shaw, K., Phillips, A., & Cooper, D. N. (2014). The Human Gene Mutation Database: building a comprehensive mutation repository for clinical and molecular genetics, diagnostic testing and personalized genomic medicine. *Hum Genet* ,*133* (1), 1-9. https://doi.org/10.1007/s00439-013-1358-4

Theunissen, T. E. J., Gerards, M., Hellebrekers, D., van Tienen, F. H., Kamps, R., Sallevelt, S., . . . Smeets, H. J. M. (2017). Selection and Characterization of Palmitic Acid Responsive Patients with an OXPHOS Complex I Defect. *Front Mol Neurosci* , *10* , 336. https://doi.org/10.3389/fnmol.2017.00336

Tinker, R. J., Lim, A. Z., Stefanetti, R. J., & McFarland, R. (2021). Current and Emerging Clinical Treatment in Mitochondrial Disease.*Mol Diagn Ther* , *25* (2), 181-206. https://doi.org/10.1007/s40291-020-00510-6

Volodarsky, M., Zilberman, U., & Birk, O. S. (2015). Novel FAM20A mutation causes autosomal recessive amelogenesis imperfecta. *Arch Oral Biol* , *60* (6), 919-922. https://doi.org/10.1016/j.archoralbio.2015.02.018

Wang, M., & Marin, A. (2006). Characterization and prediction of alternative splice sites. *Gene* , *366* (2), 219-227. https://doi.org/10.1016/j.gene.2005.07.015

Wei, X., Du, M., Li, D., Wen, S., Xie, J., Li, Y., . . . Fang, H. (2020). Mutations in FASTKD2 are associated with mitochondrial disease with multi-OXPHOS deficiency. *Hum Mutat* , *41* (5), 961-972. https://doi.org/10.1002/humu.23985

Wiel, L., Baakman, C., Gilissen, D., Veltman, J. A., Vriend, G., & Gilissen, C. (2019). MetaDome: Pathogenicity analysis of genetic variants through aggregation of homologous human protein domains. *Hum Mutat* , *40* (8), 1030-1038. https://doi.org/10.1002/humu.23798

Zheng-Bradley, X., & Flicek, P. (2017). Applications of the 1000 Genomes Project resources. *Brief Funct Genomics* , *16* (3), 163-170. https://doi.org/10.1093/bfgp/elw027

Figure titles legends

Figure 1. Segregation analysis, sanger sequence and MRI manifestation.

A. MRI image of proband. Bilateral abnormal signal in pedunculus cerebri and pons were pointed by arrow.

B. Sanger sequence of the affected family. The arrows indicate mutation sites.

C. Segregation analysis of affected individual. Rectangles indicate males, circles female, and solid circle represents affected individual. The proband was pointed out by arrow.

Figure 2. *In silico* analysis of *TMEM126B* variants.

A. Amino acid conservation analysis of exon 2 and 3, and amino acid variant tolerance in gnomAD database. Different backcolor indicates the genetic tolerance.

B. Bioinformatic analysis of allele frequency and pathogenicity prediction about two variants.

C. Putative splice sites and scores for wild-type and mutant sites predicted from ASSP.

D. Splicing regulatory protein binding motif predicted by ESE Finder for wild-type and mutants. Mutation sites are highlighted in red. NA, not available; HGMD, Human Gene Mutation Database; ACMG, the American College of Medical Genetics and Genomics.

Figure 3. The minigene splicing assays based on the pSPL3 exon trapping vector.

A. Schematic diagram of the *in vitro* minigene plasmid construction. The pSPL3 plasmid contains two exons, SD and SA. The primers were specify to exon SD and SA, respectively.

B-C. Agarose gel electrophoresis (B) and Sanger sequencing (C) for the PCR products of c.82-2A and c.82-2A>G mutant. β-actin was used as loading control.

D-E. Agarose gel electrophoresis (D) and Sanger sequencing (E) for the PCR products of c.290T and c.290dupT mutant. The c.290dupT was highlight with grey background.

F. Relative quantification of each segment of PCR product from pSPL3 control, c.290T and c.290dupT.

Figure 4. *TMEM126B* exons 2 and 3 splicing patterns in patient-derived lymphocytes.

A-B. Agarose gel electrophoresis (A) and Sanger sequencing (B) for RT-PCR products from patient and healthy control's lymphocytes, which the primers was designed at exon 1 and exon 3 respectively.

C. Schematic representation of the splicing process. The c.82-2A>G mutation resulted in premature termination at position of 58 in exon 3. V9 referred to the transcript variant 9 of *TMEM126B* (NM_001350396.2).

D-E. Agarose gel electrophoresis (D) and Sanger sequencing (E) for RT-PCR products from patient and healthy control's lymphocytes, which the primers were designed at the junction of exon 1 and 2 and exon 4 respectively to avoid amplifying additional transcripts. The mutation was highlight with grey.

F. Schematic representation of the splicing process. The c.290dupT caused a premature termination at position 100 and 101 of the two transcripts, respectively.

Figure 5. Mitochondrial functional validation in patient-derived lymphocytes.

A-B. BN-PAGE for mitochondrial complexes (A) and supercomplex (B). Asterisk indicates the incomplete assembly intermediate complex. TOM70 was used as internal loading controls.

C-E. Oxygen respiration rate (C), relative cellular ATP (D) and mitochondrial ROS content (E) of healthy control and patient-derived lymphocytes. $*p$ <0.05, $**p$ <0.01, $***p$ <0.001.

Figure 6. Overview of the *TMEM126B* variants and phenotypes.

A. The recurrent clinical phenotypes of all published literatures about *TMEM126B* mutation. Colored circles (right) indicate various compound phenotypic combination, and the histogram represents corresponding patient number (Vertical direction). The number of patients corresponding to the phenotype is indicated on the left of the graph.

B. Summary the location about *TMEM126B* mutations of all published literatures. Wathet rectangles indicates introns, primrose yellow presents exons, mazarine indicates the coding sequence.

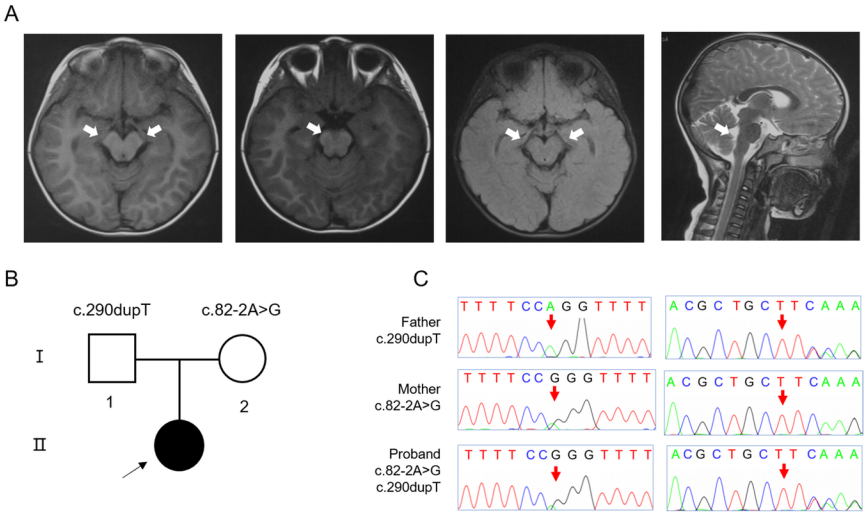

A

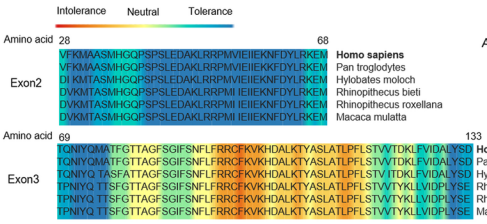

B

Nucleotide Change	c.82-2A>G	c.290dup
Amino acid Change	None	p.K98Qfs*3
Allele frequency in 1000 genomes	NA	NA
Allele frequency in gnomAD	0.0006	NA
ExAc allele frequency	NA	NA
dbSNP	NA	rs868347401
Clinvar	NA	NA
HGMD	NA	NA
ACMG	Like pathogenic	Pathogenic

C

ASSP	Putative splice site	Sequence	Score		Putative splice site	Sequence	Score
c.82-2A	Constitutive acceptor	ttttttccagGTTTTCAAGA	12.831	c.82-2A>G	None	None	None
c.290T	None	None	None	c.290dupT	Constitutive acceptor	tgctttcaagGTTAAACATG	3.532

D

ESE Finder	SRp40		SRp55	
	Motif	Score	Motif	Score
c.82-2A	TTCCAGG	3.616796	TATGGC	3.161650
c.82-2A>G	TTTCCGG	3.228096	TATGGC	3.161650
c.290T	CTTCAAG	4.040549	TGCTTC	3.831906
c.290dupT	TTTCAAG	4.397244	None	None

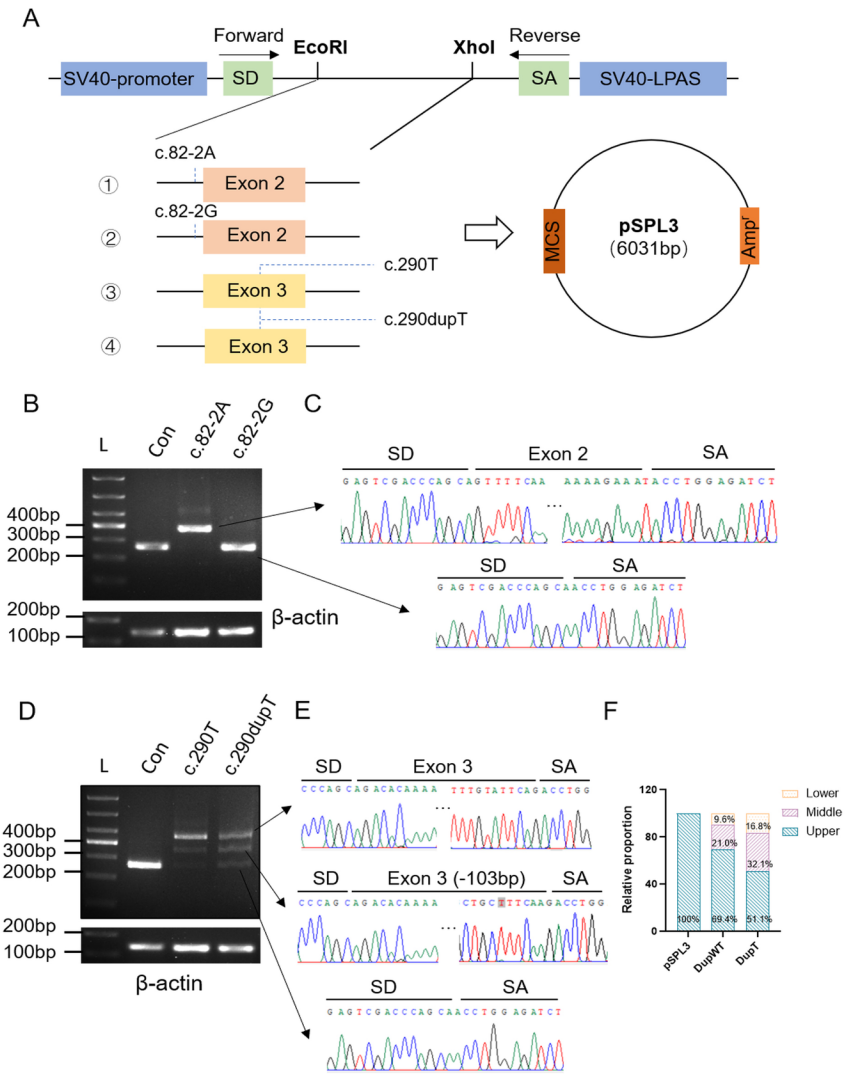

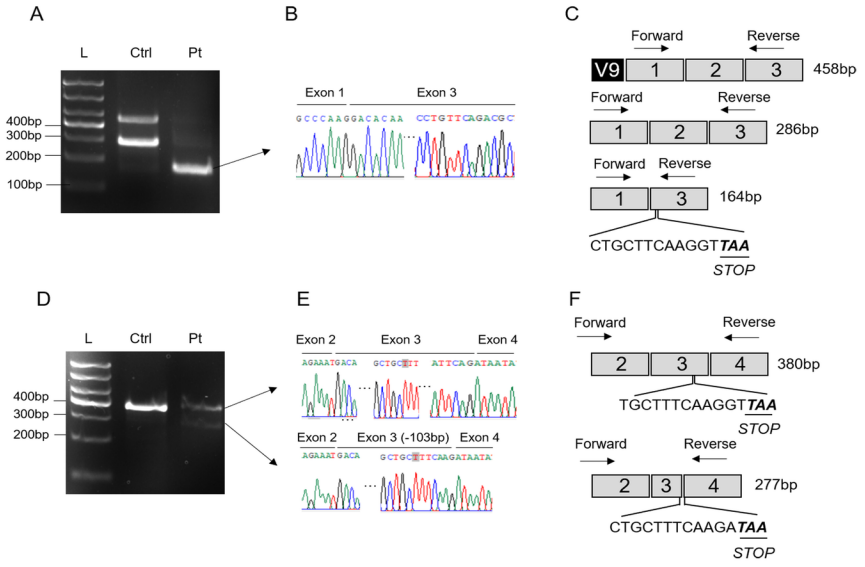

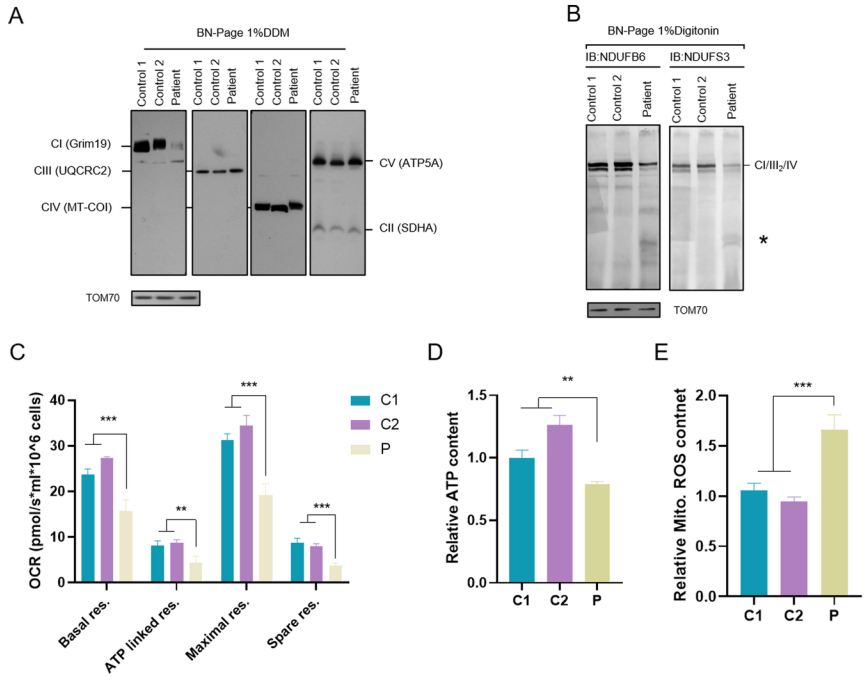

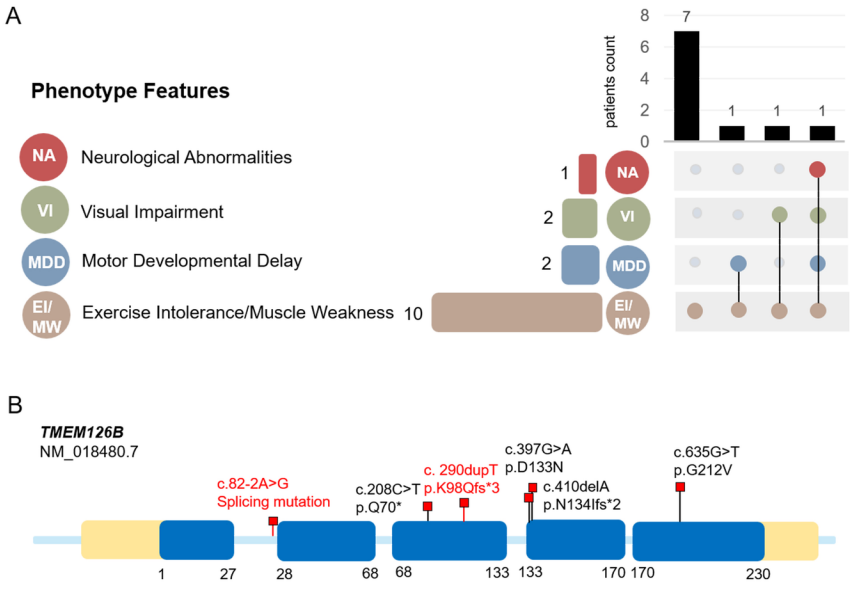

Hosted file

`Table 1.docx` available at https://authorea.com/users/493975/articles/576209-novel-biallelic-mutations-in-tmem126b-cause-splicing-defects-and-lead-to-leigh-syndrome-with-severe-complex-i-deficiency